Supporting Information

Renbaum-Wolff et al. 10.1073/pnas.1219548110

SI Materials and Methods

Composition of Secondary Organic Material from Ozonolysis of α-Pinene. Secondary organic material (SOM) formed from the ozonolysis of α-pinene is largely composed of water-soluble organic compounds. Hall and Johnston (1) determined that 63% (±27%) of the total particle mass is extractable from filters with water. Heaton et al. (2) compared the mass spectra from extracts using 100% water and 50:50 methanol:water and showed that there was little difference in the chemical composition of the two extracts. Cloud condensation measurements suggest that secondary organic material generated from the ozonolysis of α-pinene is not limited by solubility of the organic material in water under similar conditions to those used in our experiments (3). Finally, SOM produced by limonene ozonolysis, a species structurally related to α-pinene, has been shown to be nearly completely water soluble by comparing water and acetonitrile extracts (4).

Bead-Mobility Technique Details. The bead speed was converted to viscosity using a calibration curve described previously (5) (Fig. S2). The organic molecules used to generate the calibration curve had oxygen-to-carbon (O:C) elemental ratios ranging from 0.1 to 1.0, molecular weights ranging from 92 to 600 $\text{g}\cdot\text{mol}^{-1}$, surface tensions ranging from 32 to 75 $\text{mN}\cdot\text{m}^{-1}$, and contact angles with the slide substrate ranging from 58° to 95°. Within experimental uncertainty, the speed-to-viscosity relationship was independent of these parameters (5).

The characteristics of secondary organic material studied here are expected to lie within the previously studied ranges of O:C, molecular weight, surface tensions, and contact angles. For example, average O:C ratios of secondary organic particles generated from the ozonolysis of α-pinene in environmental chambers vary from 0.3 to 0.4 for the mass concentrations used (2, 6–9). Although the surface tension of secondary organic material collected in environmental chambers is largely unmeasured for the subsaturated relative humidity (RH) regime, estimates of 40–75 $\text{mN}\cdot\text{m}^{-1}$ have been made on the basis of model compounds (10–12). The myriad of compounds present in the SOM have been largely estimated to have molecular weights less than 600 $\text{g}\cdot\text{mol}^{-1}$ (9, 13, 14). Based on confocal imaging of the particles of this study, the contact angle of the SOM is between 65° and 79°.

The mean bead speeds measured using SOM (Table 1) are included in the calibration curve (Fig. S2) for comparison purposes. The overlap between the bead speeds measured with SOM and bead speeds measured with calibration standards illustrates that the current measurements are within the range of the calibration data.

Poke-Flow Equilibration Times. Similar to the bead-mobility experiments, RH inside the flow cell was initially set at 90% for 30 min after which the RH was decreased ($< 0.5\%\ \text{RH}\cdot\text{min}^{-1}$) to the experimental value, at which point the RH was held constant to allow the particles to equilibrate once more. To estimate the time for particles to come to equilibrium with the water vapor we followed the procedure outlined by Shiraiwa et al. (15), which is based on percolation theory. Equilibration times for water are expected to be significantly faster than equilibration times for larger organic molecules because small molecules like water percolate (i.e., diffuse) more rapidly through the host matrix (15). When calculating equilibration times, diffusion coefficients from Table 1 in Shiraiwa et al. (15) and the particle diameters used in the poke-flow experiments were used with equation 2 from Shiraiwa et al. (15). As mentioned above, the particle size ranging from 20 to 50 μm was used in the poke-flow experiments, although this full range was not used at each RH. Using this methodology, we estimate the equilibration time to be less than 2 h at RH ≤ 30% and less than 11 min for particles at intermediate relative humidities (40–70% RH). The time allowed for equilibration before poking ranged from 20 min at 68% RH to 2 h at ≤30% RH, which should have been sufficient for the particles to equilibrate. Even if the equilibration time is longer than predicted by percolation theory (16), it is unlikely that the particles are far from equilibrium in the poke-flow experiments, considering both the slow RH ramp down time and long equilibration times used in the experiments. At 25–30% RH there was no indication from the particle morphology that the particles were only partially dried. In addition, a strong dependence of the results on particle size was not observed, suggesting that non-equilibration between the gas and the particle was not an issue.

Simulations of Material Flow at 40–70% RH. Flow was simulated using the laminar two-phase flow moving mesh mode within the Microfluidics module of COMSOL (version 4.3a), a finite-element analysis software package. This module uses the Navier–Stokes equation including surface tension to describe transport of mass and momentum and the Arbitrary Lagrangian Eulerian (ALE) method to track the time evolution of the fluid as it flows to minimize the surface energy of the system. For the initial conditions we used a half-torus (inner diameter = 25 μm, outer diameter = 55 μm) with one of the flat faces in contact with a solid substrate. In this case we have two interfaces, labeled 1 and 2 in Fig. S4*A*. Interface 1 represents the external fluid interface and was assigned a surface tension of 75 $\text{mN}\cdot\text{m}^{-1}$ and allowed to undergo free deformation. Interface 2 represents the interface between the fluid and the solid slide substrate. This interface was allowed to deform in the X-Y plane but not in the Z direction, and the equilibrium contact angle between the surface and the fluid was assigned a value of 90° (see below for implications). Interactions between the fluid and the solid surface were described with a Navier slip wall boundary condition, with a slip length of more than an order of magnitude greater than the particle height. The effect of the slip length on the simulations is discussed below. For the fluid we assumed a density of 1.3 $\text{g}\cdot\text{cm}^{-3}$ (17–19).

Simulations were performed as a function of viscosity, and for each of these simulations we calculated the time required for the inside diameter of the torus geometry to decrease to 50% of the original diameter. We refer to this metric as $t_{(model\,flow)}$. The results of these simulations were used to generate a calibration for the relationship between $t_{(model\,flow)}$ and viscosity (Fig. S5, black solid line). This calibration curve was then used to convert $t_{(exp\,flow)}$ from Table 2 into viscosities.

Viscosities determined as described above are upper limits for the following reasons: (*a*) The calibration curve was generated with a surface tension of 75 $\text{mN}\cdot\text{m}^{-1}$, which is most likely an upper limit to the surface tensions in our experiments (10–12). If lower surface tensions were used in the simulations, the results would be lower predictions of viscosities for a given $t_{(exp\,flow)}$. (*b*) The calibration curve was generated using a contact angle of 90°, which is greater than the upper limit to the contact angle measured with a confocal microscope. If a smaller contact angle is used in the simulations, the result would be lower viscosity predictions for a given $t_{(exp\,flow)}$. (*c*) A large slip length was used in the calculations (more than an order of magnitude greater than the height of the modeled particles). This is likely an upper limit to the slip length in our experiments (20). If a smaller slip length was used, the result would be lower predictions of viscosities for a given $t_{(exp,flow)}$. (*d*) In some experiments the needle scratches the surface, resulting in reduced flows of the particle on the scratched regions (observed visually). If this process was included in the model, then the result would be lower predictions of viscosity for a given $t_{(exp,flow)}$. See annotations in Fig. S5 for the effect of decreased surface tension, decreasing contact angle, and decreasing slip length and the effect of surface scratching on the calibration curve that relates flow times to viscosities. The sensitivity of the model to changes in surface tension and contact angle was tested by comparing the $t_{(model,flow)}$ values calculated for a contact angle of 90° and a surface tension of 75 $mN\cdot m^{-1}$ (Fig. S5, solid line) to $t_{(model,flow)}$ calculated for a contact angle of 70° and a surface tension of 60 $mN\cdot m^{-1}$ (Fig. S5, dashed line). The small (20–30%) change in the predicted $t_{(model,flow)}$ values was found to be predominantly due to the change in the surface tension.

The upper limits to viscosity at 70% RH estimated from the poke-flow results are consistent with the results obtained with the bead-mobility technique (compare Table 2 and Table 1). As a further test, we performed the poke-flow technique on particles of sucrose. When sucrose particles were poked at 56% and 60% RH and half-torus geometries were formed, the resulting $t_{(exp,flow)}$ values were 5 s and 0.8 s, respectively. Using these experimental flow times and the calibration curve in Fig. S5, upper limits to the viscosity of the sucrose particles were estimated to be 1×10^4 and 6×10^4 Pa·s, at 60% and 56% RH, respectively. At 60% RH, the literature viscosity of the sucrose/water mixture is approximately 9×10^2 Pa·s. At 56% RH, the viscosity of the sucrose/water mixture is estimated to be $8\binom{+3}{-2}\times10^3$ Pa·s, based on an extrapolation of literature data using a third-degree polynomial function [Renbaum-Wolff et al. (5)].

Simulations of Material Flow at 25–30% RH. Flow in these experiments was also simulated using the laminar two-phase flow moving mesh mode within the Microfluidics module of COMSOL (version 4.3a). For the initial conditions we used a quarter of a sphere (radius = 10 μm) with one of the flat faces in contact with a solid substrate (Fig. S4*B*). In this case, there are three interfaces, labeled 1–3 in Fig. S4*B*. Interfaces 1 and 2 represent external fluid interfaces and were assigned a surface tension of 40 $mN\cdot m^{-1}$ and allowed to undergo free deformation. Interface 3 represents the interface between the fluid and the solid slide substrate. This interface was allowed to deform in the *X-Y* plane but not in the *Z* direction, and the equilibrium contact angle between the surface and the fluid was assigned a value of 90° (see below for implications). The extent of movement of the sharp edge of the particle in 8 h was independent of the equilibrium contact angle between 20° and 100°. Interactions between the fluid and the solid surface were described with a Navier slip wall boundary condition, with a slip length of 0.01*k, where k is the grid spacing of the mesh that ranged from 1 to 1.7 μm. Thus, the slip length was typically between 10 nm and 17 nm, consistent with experiments of water on hydrophobic substances at low shear rate (20). The amount of movement of the sharp edge of the particle was only weakly dependent on the slip length used, leading to less than a 10% change in the observed movement over 8 h when the slip length was varied from 1 nm to 10 μm. For the particle fluid we assumed a density of 1.3 $g\cdot cm^{-3}$ (17–19). The viscosity of the fluid was adjusted until the sharp edge at the top of the particle (viewed from above the quarter-sphere) moved by ~0.5 μm in 8 h (Fig. S4*B*). The extent of movement, 0.5 μm, was chosen because if movement of this magnitude occurs, it is clearly detectable in the microscope images.

The viscosity determined as described above is a lower bound to the viscosity in the experiments at 30–25% RH for the following reasons: (*a*) Movement of 0.5 μm in 8 h is an upper limit to the movement observed in our experiments, and (*b*) a surface tension of 40 $mN\cdot m^{-1}$ is a reasonable lower limit to the surface tension of the material in our experiment (10–12). If a higher surface tension were used in the simulations, the result would be a higher prediction of the viscosity.

To test the approach described above for extracting lower limits to viscosities, the poke-flow technique was performed on particles of raffinose at 30% RH. According to Zobrist et al. (21), raffinose passes through a relative humidity-induced glass transition at ~53% RH at room temperature. At 30% RH, therefore, raffinose particles are expected to be in a glassy state, with viscosities $\geq 10^{12}$ Pa·s. The poke-flow experiment was performed on raffinose particles at 30% RH and the particles shattered into well-defined pieces with sharp edges. Movement was less than 0.5 μm in 8 h. The lower limit of the viscosity estimated with the quarter-sphere COMSOL model discussed above was 5×10^8 Pa·s, which is consistent with the established viscosity ($\geq 10^{12}$ Pa·s) for this material.

We also carried out simulations using other geometries to determine whether the predicted lower bounds of the viscosities were sensitive to the initial geometry. For example, we carried out simulations using (*a*) a 2D square as the initial geometry with lengths for the sides set to 20 μm and (*b*) a 3D cylinder with a height and radius of 20 μm and 10 μm, respectively. In these two cases no interactions with a stationary surface were considered. Both the 2D square model and the 3D cylinder model resulted in 0.5 μm movement in 8 h when a viscosity of 1×10^9 Pa·s was used, suggesting the quarter-sphere model used herein provides the most conservative lower limit to the viscosity of these models.

Viscosity Prediction Using Mixing Rules. A common approach to estimating the viscosity of mixtures (η_{mix}) is to apply mixing rules to the viscosities of the pure components of the mixture on the basis of experimental data and/or theory. Among the simplest of mixing rules for complex mixtures was first proposed by Arrhenius (1885) and considered the mole fraction of each component (x_i) and the viscosity of each pure component (η_i) (22):

$$log\,(\eta_{mix}) = \sum_{i=1}^{n} x_i log\,(\eta_i). \qquad \textbf{[S1]}$$

Eq. **S1** was later modified by Grunberg and Nissan (22) to include a group interaction parameter, *G*, accounting for nonideality of the complex mixture, the result of which was a closer fit to the experimental data (22):

$$log\,(\eta_{mix}) = \sum_{i=1}^{n} x_i log\,(\eta_i) + \sum_{i=1}^{n}\sum_{j=1}^{n} x_i x_j G_{i,j}. \qquad \textbf{[S2]}$$

If the interaction parameter, $G_{i,j}$, between the SOM components is small, and the mole fraction of water is a linear function of RH, Eq. **S2** predicts a linear dependence of $log(\eta_{SOM-H_2O})$ vs. RH, roughly consistent with what is observed in Fig. 2, where $log(\eta_{SOM-H_2O})$ is the viscosity of the SOM–water mixture. Any deviation from linearity, for instance between 30% and 40% RH, may be due to nonideality and/or a gel or glass transitions in that RH regime. Accurate predictions of viscosities in aqueous mixtures may require an additional interaction term in Eq. **S2**, the result of which is further nonlinearity in the plots of $log\,(\eta_{mix})$ [or $log\,(\eta_{SOM-H_2O})$] (23).

It should be noted that the use of equations such as Eqs. **S1** and **S2** for mixtures containing components with very large differences in the viscosities of the pure components is not well established and they are used here only for a first-order approximation of the trend in the viscosity expected with changing RH. However, other formulations modeling the viscosity of specific polar mixtures such as sucrose–water mixtures predict a linear correlation between $log\,(\eta_{mix})$ and concentration even with a large difference in pure component viscosities (24).

1. Hall WA IV, Johnston MV (2011) Oligomer content of α-pinene secondary organic aerosol. *Aerosol Sci Technol* 45:37–45.
2. Heaton KJ, Sleighter RL, Hatcher PG, Hall WA, 4th, Johnston MV (2009) Composition domains in monoterpene secondary organic aerosol. *Environ Sci Technol* 43(20):7797–7802.
3. King SM, Rosenoern T, Chen Q, Martin ST (2009) Increased cloud activation potential of secondary organic aerosol for atmospheric mass loadings. *Atmos Chem Phys* 9:2959–2972.
4. Bateman AP, Nizkorodov SA, Laskin J, Laskin A (2010) High-resolution electrospray ionization mass spectrometry analysis of water-soluble organic aerosols collected with a particle into liquid sampler. *Anal Chem* 82(19):8010–8016.
5. Renbaum-Wolff L, Grayson JW, Bertram AK (2013) Technical note: New methodology for measuring viscosities in small volumes characteristic of environmental chamber particle samples. *Atmos Chem Phys* 13:791–802.
6. Chen Q, Liu Y, Donahue NM, Shilling JE, Martin ST (2011) Particle-phase chemistry of secondary organic material: Modeled compared to measured O:C and H:C elemental ratios provide constraints. *Environ Sci Technol* 45(11):4763–4770.
7. Shilling JE, et al. (2009) Loading-dependent elemental composition of α-pinene SOA particles. *Atmos Chem Phys* 9:771–782.
8. Aiken AC, et al. (2008) O/C and OM/OC ratios of primary, secondary, and ambient organic aerosols with high-resolution time-of-flight aerosol mass spectrometry. *Environ Sci Technol* 42(12):4478–4485.
9. Putman AL, et al. (2012) Ultrahigh-resolution FT-ICR mass spectrometry characterization of α-pinene ozonolysis SOA. *Atmos Environ* 46:164–172.
10. Huff Hartz KE, et al. (2006) Cloud condensation nuclei activation of limited solubility organic aerosol. *Atmos Environ* 40:605–617.
11. Hyvärinen A-P, et al. (2006) Surface tensions and densities of oxalic, malonic, succinic, maleic, malic, and cis-pinonic acids. *J Chem Eng Data* 51:255–260.
12. Tuckermann R, Cammenga HK (2004) The surface tension of aqueous solutions of some atmospheric water-soluble organic compounds. *Atmos Environ* 38:6135–6138.
13. Gao S, et al. (2004) Low-molecular-weight and oligomeric components in secondary organic aerosol from the ozonolysis of cycloalkenes and α-pinene. *J Phys Chem A* 108:10147–10164.
14. Gao Y, Hall WA, Johnston MV (2010) Molecular composition of monoterpene secondary organic aerosol at low mass loading. *Environ Sci Technol* 44(20):7897–7902.
15. Shiraiwa M, Ammann M, Koop T, Pöschl U (2011) Gas uptake and chemical aging of semisolid organic aerosol particles. *Proc Natl Acad Sci USA* 108(27):11003–11008.
16. Bones DL, Reid JP, Lienhard DM, Krieger UK (2012) Comparing the mechanism of water condensation and evaporation in glassy aerosol. *Proc Natl Acad Sci USA* 109(29):11613–11618.
17. Saathoff H, et al. (2009) Temperature dependence of yields of secondary organic aerosols from the ozonolysis of α-pinene and limonene. *Atmos Chem Phys* 9:1551–1577.
18. Ng NL, et al. (2006) Contribution of first- versus second-generation products to secondary organic aerosols formed in the oxidation of biogenic hydrocarbons. *Environ Sci Technol* 40(7):2283–2297.
19. Chen X, Hopke PK (2009) Secondary organic aerosol from α-pinene ozonolysis in dynamic chamber system. *Indoor Air* 19(4):335–345.
20. Churaev NV, Sobolev VD, Somov AN (1984) Slippage of liquids over lyophobic solid surfaces. *J Colloid Interface Sci* 97:574–581.
21. Zobrist B, Marcolli C, Pedernera D, Koop T (2008) Do atmospheric aerosols form glasses? *Atmos Chem Phys* 8:5221–5244.
22. Grunberg L, Nissan AH (1949) Mixture law for viscosity. *Nature* 164(4175):799–800.
23. Marczak W, Adamczyk N, Lezniak M (2012) Viscosity of associated mixtures approximated by the Grunberg-Nissan model. *Int J Thermophys* 33:680–691.
24. Longinotti MP, Corti HR (2008) Viscosity of concentrated sucrose and trehalose aqueous solutions including the supercooled regime. *J Phys Chem Ref Data* 37:1503–1515.

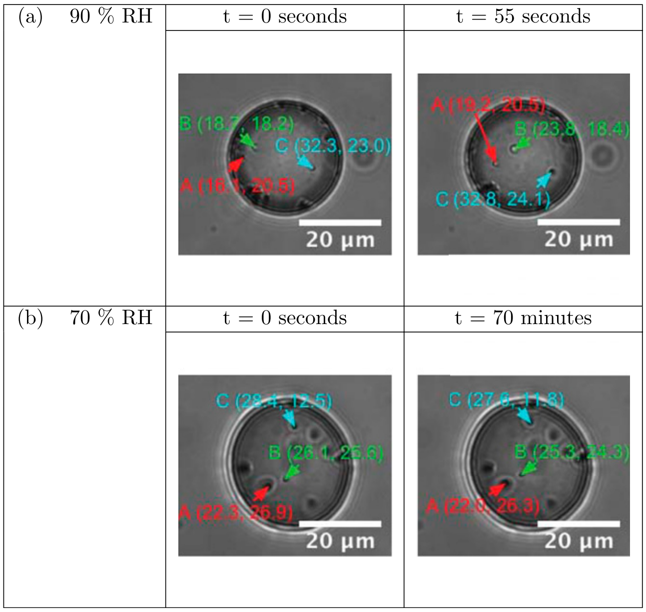

Fig. S1. Images from the "bead-mobility" studies. (*A* and *B*) Images recorded at 90% RH (*A*) and at 70% RH (*B*). Indicated are different beads monitored in the experiments and the *x*-*y* coordinates of the beads.

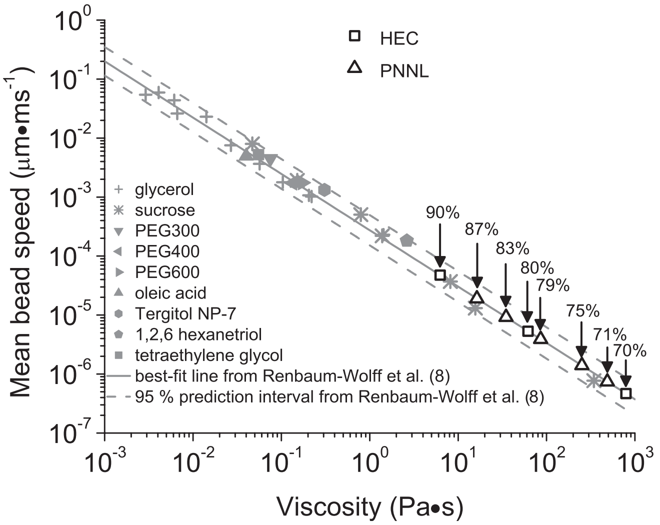

Fig. S2. Calibration curve and 95% prediction limits (gray solid and dashed lines, respectively) from Renbaum-Wolff et al. (5) that relate mean bead speeds to viscosity. Shown are the various standards used to generate the calibration curve (gray symbols) and the SOM results, which were obtained by using the best-fit function from the calibration to determine the viscosity of the SOM material (black data points). HEC, Harvard Environmental Chamber; PNNL, Pacific Northwest National Laboratory Continuous-Flow Environmental Chamber; PEG300, PEG400, and PEG600, polyethylene glycol with average molecular weights of 300, 400, and 600 g·mol^{-1}; and Tergitol NP-7, α-(4-nonylphenyl)-ω-hydroxy-poly(oxy-1,2-ethanediyl), branched.

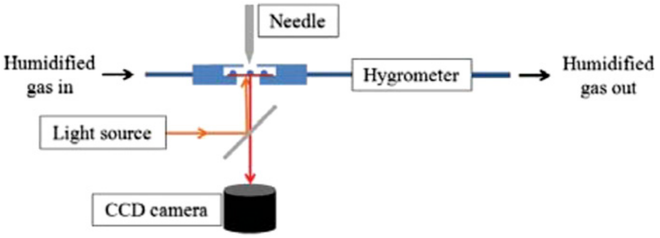

Fig. S3. Diagram of the apparatus used in the “poke-flow” experiments. Relative humidity control in the apparatus is achieved by adjusting the relative humidity of the flow gas, using a mixture of wet and dry flows. The dew point is measured with a dew point hygrometer, and the temperature of the flow cell is measured using a thermocouple probe. A small hole in the top of the cell allows particles to be poked while the particles are observed using an inverted reflectance microscope.

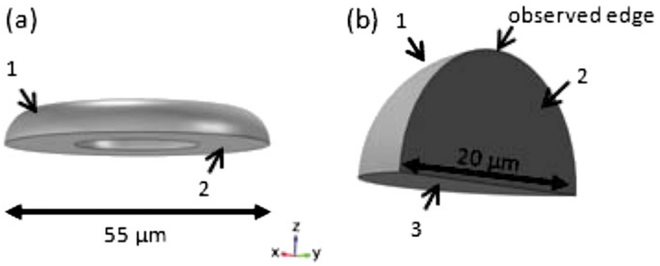

Fig. S4. (*A*) Details of half-torus model used to simulate the flow in experiments with RH values between 40% and 70%. In *A*, surface 1 represents the external fluid interface and was assigned a surface tension of 75 mN·m^{-1}, and surface 2 represents the particle–substrate interface, which was represented as a Navier-slip boundary with a slip height greater than the particle height. (*B*) Details of quarter-sphere model used to simulate the flow in experiments with RH values ≤30% RH. In *B*, surfaces 1 and 2 represent the external fluid interfaces that were assigned a surface tension of 40 mN·m^{-1}, and surface 3 represents the particle–substrate interface, which was represented as a Navier-slip boundary with a slip height of 10–17 nm.

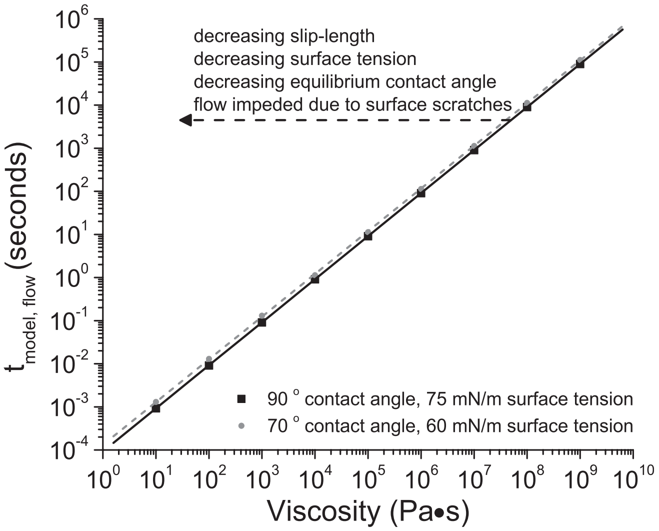

Fig. S5. Calibration line from COMSOL simulations (black solid line). In the simulations used to generate this calibration a surface tension of 75 mN·m^{-1} and contact angle of 90° were used and interactions between the fluid and a stationary surface/substrate were not considered. The annotation illustrates how the calibration line would shift if a smaller surface tension, a smaller equilibrium contact angle, smaller slip length, and/or surface scratching were included in the model. An example line constructed with lower surface tension (60 mN·m^{-1}) and lower contact angle (70°) is given to display the sensitivity of the model to these parameters (gray dashed line).

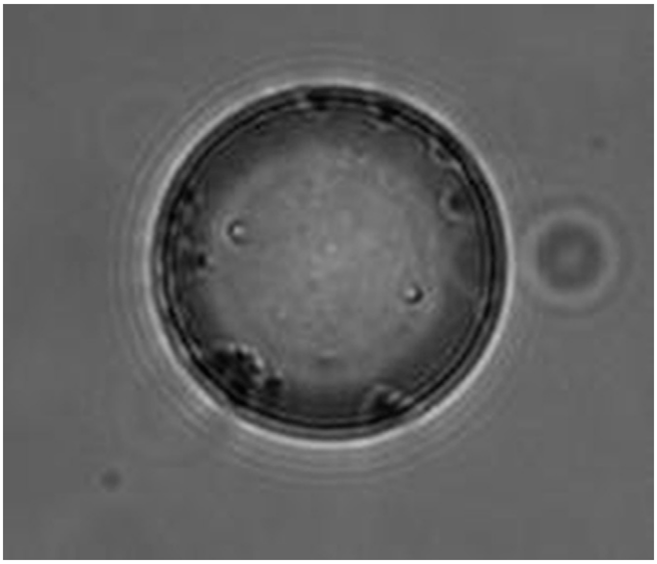

Movie S1. Beads moving within a particle of water-soluble SOM from the ozonolysis of α-pinene. Time scale: 1/10 × real time.

Movie S1

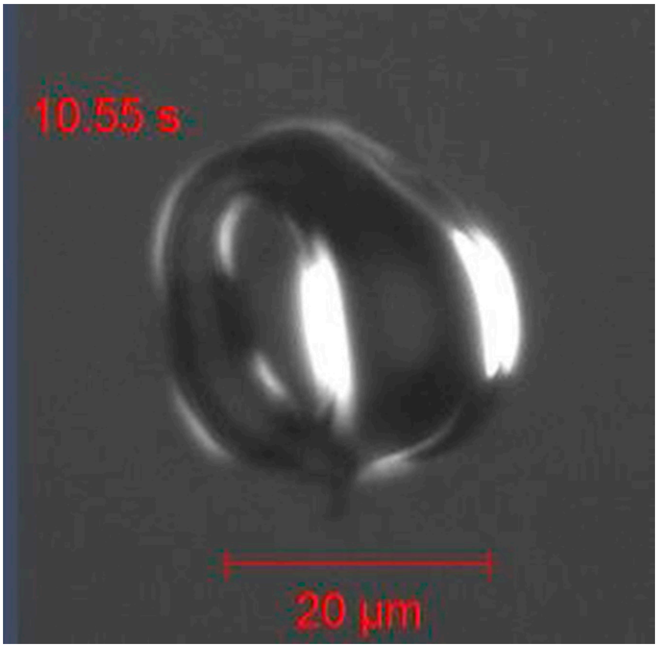

Movie S2. Movie of particle being poked at 70% RH. Length scales and elapsed time are included in the individual frames. Timescale: real time. The sample was collected from the Harvard Environmental Chamber, using a quartz fiber filter.

Movie S2

Movie S3. Movie of fluid flow simulated with COMSOL. Starting geometry is a half-torus ring with viscosity = 1.0×10^6 Pa·s, surface tension = 75 mN·m^{-1}, particle density = 1.3 g·cm^{-3}, and a slip length of >10 times the torus height. Timescale: 1/5 × real time.

Movie S3

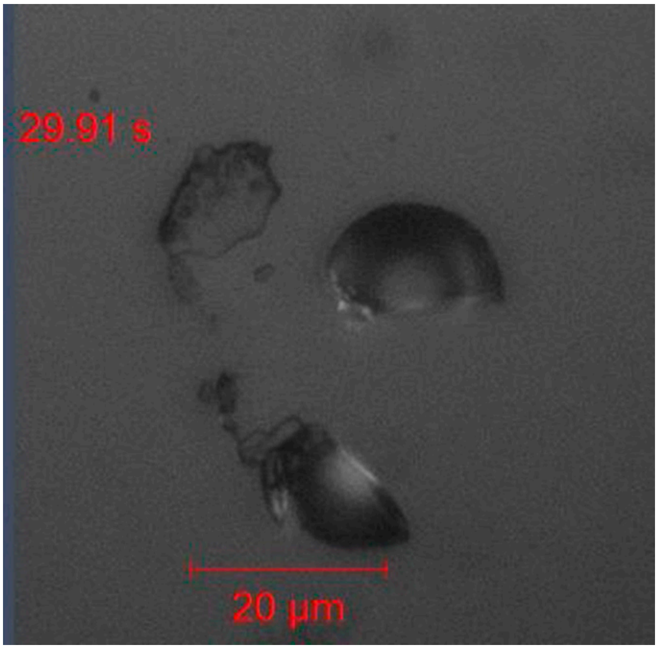

Movie S4. Movie of particle being poked at 30% RH. Length scales and elapsed time are included in the individual frames. Timescale: real time. The sample was collected from the Harvard Environmental Chamber, using a quartz fiber filter.

Movie S4

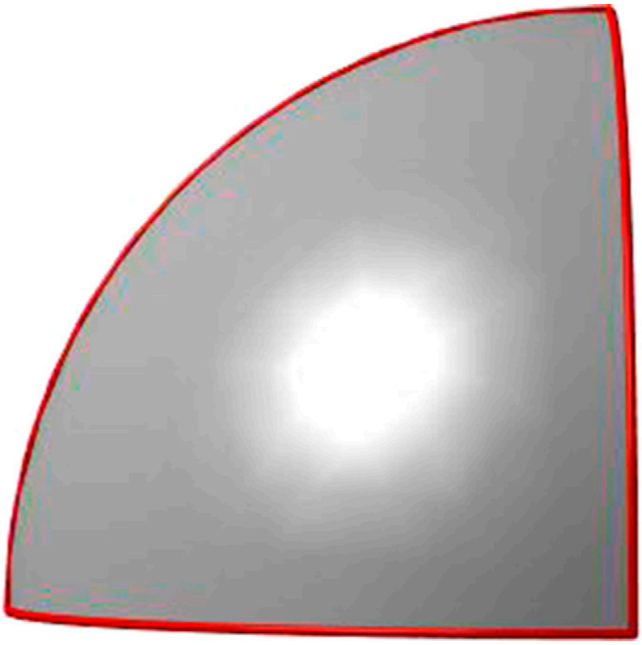

Movie S5. Simulation of fluid flow with COMSOL, assuming a starting geometry of one-quarter of a sphere with one of the flat sides in contact with a stationary surface. Timescale: 1/500 × real time. Fluid viscosity = 5×10^{8} Pa·s, surface tension = 40 mN·m^{-1}, particle density = 1.3 g·cm^{-3}, and a slip length of 10–17 nm were assumed in this simulation.

Movie S5